# Quantum Monte Carlo Calculations with Chiral Effective Field Theory Interactions: Developments and a Recent Application

**Joel E. Lynn**

*Institut für Kernphysik, Technische Universität Darmstadt, 64289, Darmstadt, Germany*
*ExtreMe Matter Institute EMMI, GSI Helmholtzzentrum für Schwerionenforschung GmbH, 64291 Darmstadt, Germany*

**Abstract**

Quantum Monte Carlo methods are among the most accurate nuclear many-body methods available. Chiral effective field theory presents a systematic way to derive nuclear Hamiltonians from effective field theory with the same symmetries as low-energy quantum chromodynamics. Here we describe the developments that have led to the combination of these two powerful approaches, a recent application, and prospects for the future.

**Keywords:** *Nuclear interactions; ab initio methods*

## 1 Introduction

Low-energy nuclear physics sits in a privileged position, connecting many different research areas including (among others) nuclear structure, fundamental symmetries, and nuclear astrophysics. In each of these areas of inquiry, there are large open questions. For example, in nuclear structure, we might ask: What are the limits of existence of the nuclear chart? How far can *ab initio* calculations be pushed? How can we build a coherent framework for describing nuclei, nuclear matter, and nuclear reactions?

While quantum chromodynamics (QCD) is ultimately responsible for strong interactions, at low energies most applicable to many phenomenon in nuclear physics, the most relevant degrees of freedom are baryons and mesons, specifically nucleons and pions. But even choosing to work with these simplified degrees of freedom over the fundamental degrees of freedom (quarks and gluons), nuclear systems still present a significant challenge because they are strongly interacting many-body systems.

Two questions must be addressed: 1) How do we solve the many-body Schrödinger equation,

$$H|\Psi_0\rangle = E_0|\Psi_0\rangle? \tag{1}$$

and 2) Where should we take the Hamiltonian $H$? There are, of course, many answers possible to both questions. In this brief overview, we will discuss one possible answer

*Proceedings of the International Conference 'Nuclear Theory in the Supercomputing Era — 2016' (NTSE-2016), Khabarovsk, Russia, September 19–23, 2016. Eds. A. M. Shirokov and A. I. Mazur. Pacific National University, Khabarovsk, Russia, 2018, p. 140.*

*http://www.ntse-2016.khb.ru/Proc/Lynn.pdf.*

set: 1) Quantum Monte Carlo (QMC) methods, and 2) Chiral effective field theory (EFT). Low-energy nuclear theory can make significant contributions to many areas of research and the combination of QMC methods and chiral EFT interactions is an important piece of the puzzle.

## 2 Quantum Monte Carlo methods

Quantum Monte Carlo methods are among the most accurate many-body methods in use in nuclear physics. They include the Variational Monte Carlo (VMC) method, the Green's Function Monte Carlo (GFMC) method, and the Auxiliary-Field Diffusion Monte Carlo (AFDMC) method.

The first method relies on the Rayleigh–Ritz variational principle to establish an upper bound for the ground-state energy. In a few sentences, the idea is as follows. One makes an educated guess for the many-body wave function $|\Psi_T(\{c_i\})\rangle$, which is known as the trial wave function and which depends on some set of adjustable parameters $\{c_i\}$. A set of random configurations is generated $\{\mathbf{R}_i\}$, with $\mathbf{R}_i = \{\mathbf{r}_1, \mathbf{r}_2, \ldots, \mathbf{r}_A\}_i$, a set of $3A$ coordinates for the $A$ nucleons. Then, the Metropolis algorithm is used to generate new configurations $\{\mathbf{R}'_i\}$ based on the probability $P = \frac{|\Psi_T(\mathbf{R}')|^2}{|\Psi_T(\mathbf{R})|^2}$, suppressing the dependence on the variational parameters. Ultimately, what this yields is a set of configurations (often called "walkers"), which are distributed according to the square of the trial wave function. At this point, the variational principle is invoked and the expectation value of the Hamiltonian in this state is an upper bound to the ground-state energy:

$$\frac{\langle\Psi_T|H|\Psi_T\rangle}{\langle\Psi_T|\Psi_T\rangle} > E_0. \tag{2}$$

Searches are performed over parameter sets $\{c_i\}$ minimizing the energy.

In addition to the intrinsic value of VMC calculations, they also serve as the starting point for the latter two QMC methods, which belong to a class of so-called "diffusion" Monte Carlo methods. These solve the many-body Schrödinger equation,

$$H|\Psi_0\rangle = E_0|\Psi_0\rangle, \tag{3}$$

for a system described by a Hamiltonian $H$, with ground state $|\Psi_0\rangle$ and energy $E_0$, by using the deceptively simple-looking evolution operator

$$\lim_{\tau\to\infty} \mathrm{e}^{-H\tau}|\Psi_T\rangle \to |\Psi_0\rangle, \tag{4}$$

for an initial "trial" state $|\Psi_T\rangle$. (The operator $\mathrm{e}^{-H\tau}$ is known by many names including the imaginary-time diffusion operator, the Euclidean-time projection operator, and the imaginary-time propagator.) To see how this works, expand the trial state in a complete set of eigenstates of the Hamiltonian:

$$|\Psi_T\rangle = \sum_{n=0}^{\infty} |\Psi_n\rangle\langle\Psi_n|\Psi_T\rangle = \sum_{n=0}^{\infty} \alpha_n|\Psi_n\rangle. \tag{5}$$

One tries to ensure that the overlap with the ground state is maximal: $\alpha_0 \gg \alpha_{n\neq 0}$, but inevitably, there is some contamination in the trial state from higher excited

states. Now propagate in imaginary time:

$$\lim_{\tau\to\infty} \mathrm{e}^{-(H-E_T)\tau} \sum_{n=0}^{\infty} \alpha_n |\Psi_n\rangle = \lim_{\tau\to\infty} \mathrm{e}^{-(H-E_T)\tau} \sum_{n=0}^{\infty} \alpha_n \mathrm{e}^{-(E_n-E_T)\tau} |\Psi_n\rangle$$
$$= \lim_{\tau\to\infty} \mathrm{e}^{-(E_0-E_T)\tau} \left( \alpha_0 |\Psi_0\rangle + \sum_{n>0}^{\infty} \alpha_n \mathrm{e}^{-(E_n-E_0)\tau} |\Psi_n\rangle \right). \quad (6)$$

Eq. (6) introduces the trial energy $E_T$, which controls the normalization, and makes the remainder of the argument clearer. It is typically chosen equal to the ground-state energy (though it need not be). In the second line, an overall exponential has been factored out. Now, given that $E_T \sim E_0$ and $E_n > E_0$, under the limit, the only term that remains is the ground state:

$$\lim_{\tau\to\infty} \mathrm{e}^{-(H-E_T)\tau} |\Psi_T\rangle = \alpha_0 |\Psi_0\rangle. \quad (7)$$

## 3 Chiral effective field theory

Ultimately QCD is responsible for the properties of strongly interacting nuclear matter. The Lagrangian of QCD for the two lightest quarks, $u$ and $d$, can be written as

$$\mathcal{L}_{\mathrm{QCD}} = -\frac{1}{2g^2} \mathrm{tr}\{G_{\mu\nu} G^{\mu\nu}\} + \mathrm{i}\bar{q}\gamma^{\mu} D_{\mu} q - \bar{q}\mathcal{M} q, \quad (8)$$

where $q$ ($\bar{q}$) collects the quark (antiquark) fields, $G_{\mu\nu}$ is the nonabelian gluon field strength tensor, $g$ the coupling constant, $D_{\mu}$ a gauge covariant derivative, and $\mathcal{M}$ the mass matrix. In the massless limit $\mathcal{M} \to 0$, the Lagrangian exhibits a chiral symmetry where the fields transform independently under left- and right-handed SU(2) rotations. This is the chiral symmetry of low-energy QCD. Now one can follow the Weinberg's prescription to write down the most general Lagrangian in the low-energy degrees of freedom (pions and nucleons) consistent with the important symmetries of the underlying theory (chiral symmetry),

$$\mathcal{L}_{\mathrm{eff}} = \mathcal{L}_{\pi\pi} + \mathcal{L}_{\pi N} + \mathcal{L}_{NN}. \quad (9)$$

Once a power-counting method is specified, then one can order the Lagrangians in powers of a small parameter $Q/\Lambda$, where $Q$ is some typical momentum scale in low-energy nuclear physics, e. g., the pion mass, and $\Lambda$ is some hard scale naively of the order of the chiral symmetry breaking scale $\Lambda \sim 1$ GeV. For example, the nucleon-nucleon Lagrangian can be written as a sum of terms $\mathcal{L}_{NN}^{(n)}$ with $n$ signifying the order $(Q/\Lambda)^n$:

$$\mathcal{L}_{NN} = \mathcal{L}_{NN}^{(0)} + \mathcal{L}_{NN}^{(2)} + \mathcal{L}_{NN}^{(3)} + ... \quad (10)$$

From such an effective Lagrangian, a nuclear potential can be extracted, which also obeys the same ordering:

$$V_{NN} = V_{NN}^{(0)} + V_{NN}^{(2)} + V_{NN}^{(3)} + ... \quad (11)$$

The advantages of this approach are several. All of the long-range physics is governed explicitly by one- and multi-pion exchanges. The short-range physics is captured in

contact operators multiplied by unknown low-energy constants (LECs) that must be fitted to data. And importantly, many-body forces and electroweak currents enter in a systematic way. For example, the three-nucleon interaction enters first at the order $(Q/\Lambda)^3$ (also known as next-to-next-to-leading order or N$^2$LO). For more details see Refs. [1, 2].

An important detail from the point of view of QMC methods, is that most chiral EFT interactions are nonlocal: $\langle \mathbf{r}|V|\mathbf{r}'\rangle = V(\mathbf{r},\mathbf{r}')$. While some work has been done to include nonlocal potentials in QMC methods [3, 4], in practice, QMC methods require local potentials with $\langle \mathbf{r}|V|\mathbf{r}'\rangle = V(\mathbf{r})\,\delta^{(3)}(\mathbf{r}-\mathbf{r}')$. However, recently an equivalent formulation has been derived that allows for the construction of local interactions from chiral EFT up to N$^2$LO [5,6], which has been implemented and tested in GFMC calculations of light nuclei and AFDMC calculations of neutron matter [7,8]. References [5–8] contain the detailed derivation of the local two- and three-nucleon interactions from chiral EFT, here we briefly summarize the underlying ideas.

If $\mathbf{q} \equiv \mathbf{p} - \mathbf{p}'$ is the momentum transfer in terms of the incoming and outgoing relative momenta $\mathbf{p}$ and $\mathbf{p}'$, and $\mathbf{k} \equiv \frac{1}{2}(\mathbf{p} + \mathbf{p}')$ is the momentum transfer in the exchange channel, then any functional dependence on $\mathbf{k}$ will lead to a nonlocal interaction, whereas the $\mathbf{q}$ dependence Fourier transforms to a local interaction. Then, the two sources of nonlocality come from 1) the regulator function (used to regulate high-momentum components of the interaction) and 2) the choice of operators in the contact sector of the interaction. 1) The typical regulator function used in momentum space is $f(p) = \mathrm{e}^{-(p/\Lambda)^n}$, with $\Lambda$ being a cutoff scale, and $n > 2$ is some appropriate power. Then,

$$V(\mathbf{p},\mathbf{p}') \to V(\mathbf{p},\mathbf{p}')\, f(p)\, f(p'). \tag{12}$$

In short, even if $V(\mathbf{p},\mathbf{p}')$ were such that it would Fourier transform to a local interaction, the regulation scheme of Eq. (12) spoils this. The solution is to regulate in the coordinate space in a local way: $f(r) \propto \mathrm{e}^{-(r/R_0)^4}$, where $R_0 = 1.0$–$1.2$ fm serves as the coordinate-space cutoff (approximately equivalent to 500–400 MeV, respectively). 2) At leading order (LO) in Weinberg power counting, the nuclear interaction consists of the one-pion-exchange potential, and (in principle) four possible momentum-independent contact operators: $\{\mathbb{1},\, \boldsymbol{\tau}_1\cdot\boldsymbol{\tau}_2,\, \boldsymbol{\sigma}_1\cdot\boldsymbol{\sigma}_2,\, \boldsymbol{\sigma}_1\cdot\boldsymbol{\sigma}_2\,\boldsymbol{\tau}_1\cdot\boldsymbol{\tau}_2\}$. However, nucleons are fermions and obey the Pauli exclusion principle. This means that we will ultimately be taking matrix elements between antisymmetric states, and an antisymmetrized potential $V \to \mathcal{A}V$ will give equivalent results. Under this antisymmetrization operation, it can be shown that at LO, only two of four contact operators are linearly independent. This same freedom exists at the next-to-leading order (NLO) where out of fourteen possible momentum-dependent operators only seven are linearly independent under the antisymmetrization operation. This "Fierz" freedom can be exploited to choose a set of (mostly) local operators. (The exception comes from one operator proportional to $\mathbf{q}\times\mathbf{k}$, but this is none other than the spin-orbit operator, which has long been included explicitly in QMC methods and causes no significant difficulty.) At the next-to-next-to-next-to-leading order (N$^3$LO), this Fierz freedom is insufficient to remove all $\mathbf{k}$-dependent operators, and so a maximally local set will have to be selected. See Ref. [9] for a similar approach. It is possible that the remaining nonlocal operators are "small" and can be included perturbatively in QMC methods.

### 3.1 Three-nucleon interactions

An important consideration, both from the point of view of agreement with experimental nuclear structure and from the point of view of consistency in the power counting, is the inclusion of three-nucleon interactions that appear at N$^2$LO. Again, we refer the interested reader to details provided in Refs. [6,8], but briefly summarize the important points here. There are three Feynman diagrams contributing to the three-nucleon interaction at N$^2$LO in Weinberg power counting, pictured in Fig. 1.

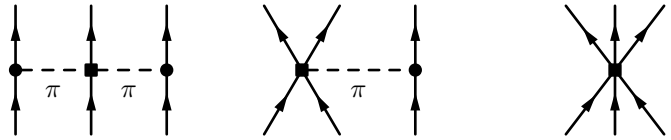


Figure 1: Feynman diagrams contributing to the three-nucleon interaction at N$^2$LO. Solid lines are nucleons, dashed lines are pions.

The Fourier transform of the first diagram has two parts. The first, which depends on the LEC $c_1$, is an $s$-wave two-pion exchange, which bears resemblance to the $a'$ term of the Tucson–Melbourne interaction [10]. The second, which depends on the LECs $c_3$ and $c_4$, is a $p$-wave two-pion exchange, which bears resemblance to the Fujita–Miyazawa interaction [11]. (There are short-range structures that arise in the Fourier transforms of the $c_3$ and $c_4$ interactions, which we retain explicitly.)

The second diagram proportional to the LEC $c_D$ leads, under Fourier transform with a finite regulator, to two possible interactions, which in the infinite momentum-space cutoff limit would be identical. These two interactions differ in their short-distance structure:

$$V_{D1} \propto \sum_{i<j<k} \sum_{\rm cyc} (\boldsymbol{\tau}_i \cdot \boldsymbol{\tau}_k) \times \left[ X_{ik}(\mathbf{r}_{kj})\, \delta_{R_{3N}}(\mathbf{r}_{ij}) + X_{ik}(\mathbf{r}_{ij})\, \delta_{R_{3N}}(\mathbf{r}_{kj}) - \frac{8\pi}{m_\pi^2}\, \boldsymbol{\sigma}_i \cdot \boldsymbol{\sigma}_k\, \delta_{R_{3N}}(\mathbf{r}_{ij})\, \delta_{R_{3N}}(\mathbf{r}_{kj}) \right]; \quad (13)$$

$$V_{D2} \propto \sum_{i<j<k} \sum_{\rm cyc} (\boldsymbol{\tau}_i \cdot \boldsymbol{\tau}_k) \times \left[ X_{ik}(\mathbf{r}_{ik}) - \frac{4\pi}{m_\pi^2}\, \boldsymbol{\sigma}_i \cdot \boldsymbol{\sigma}_k\, \delta_{R_{3N}}(\mathbf{r}_{ik}) \right] \big( \delta_{R_{3N}}(\mathbf{r}_{ij}) + \delta_{R_{3N}}(\mathbf{r}_{kj}) \big). \quad (14)$$

Here, $\boldsymbol{\sigma}$ ($\boldsymbol{\tau}$) is a Pauli spin (isospin) matrix, $m_\pi$ is the pion mass, $X_{ij}(\mathbf{r}) = [S_{ij}(\mathbf{r})\, T(r) + \boldsymbol{\sigma}_i \cdot \boldsymbol{\sigma}_j] Y(r)$ is the coordinate-space pion propagator with $S_{ij}(\mathbf{r}) = 3\boldsymbol{\sigma}_i \cdot \hat{\mathbf{r}}\, \boldsymbol{\sigma}_j \cdot \hat{\mathbf{r}} - \boldsymbol{\sigma}_i \cdot \boldsymbol{\sigma}_j$ being the tensor operator, the tensor and Yukawa functions are $T(r) = 1 + 3/(m_\pi r) + 3/(m_\pi r)^2$ and $Y(r) = \mathrm{e}^{-m_\pi r}/r$, and $\delta_{R_{3N}}(\mathbf{r}) \propto \mathrm{e}^{-(r/R_{3N})^4}$ is the short-range regulated delta function with cutoff $R_{3N}$. In the above expressions, the pion-exchange-range interactions ($\propto Y$) are multiplied by a long-range regulator of the form $1 - \mathrm{e}^{-(r/R_{3N})^4}$. We take $R_{3N} = R_0$, where $R_0$ is the cutoff used in the two-nucleon interaction. The sums $\sum_{i<j<k}$ and $\sum_{\rm cyc}$ are taken over all triples in a nucleus and over all cyclic permutations of the labels $i, j, k$, respectively. It is straightforward

to see that in the limit of $R_{3N} \to 0$, that is, the limit where $\delta_{R_{3N}}(\mathbf{r}) \to \delta(\mathbf{r})$, equations (13) and (14) agree.

The third diagram proportional to the LEC $c_E$ leads to an interaction of the following form:

$$V_E \propto \sum_{i<j<k} \sum_{\text{cyc}} O_{ijk}\, \delta_{R_{3N}}(\mathbf{r}_{ij})\, \delta_{R_{3N}}(\mathbf{r}_{kj}), \tag{15}$$

where, in principle, the Fierz freedom as in the two-nucleon sector allows the choice of the operator $O_{ijk}$ as one from the set

$$\{\mathbb{1}, \boldsymbol{\sigma}_i{\cdot}\boldsymbol{\sigma}_j, \boldsymbol{\tau}_i{\cdot}\boldsymbol{\tau}_j, \boldsymbol{\sigma}_i{\cdot}\boldsymbol{\sigma}_j\, \boldsymbol{\tau}_i{\cdot}\boldsymbol{\tau}_j, \boldsymbol{\sigma}_i{\cdot}\boldsymbol{\sigma}_j\, \boldsymbol{\tau}_i{\cdot}\boldsymbol{\tau}_k, [(\boldsymbol{\sigma}_i \times \boldsymbol{\sigma}_k)\cdot\boldsymbol{\sigma}_k][(\boldsymbol{\tau}_i \times \boldsymbol{\tau}_k)\cdot\boldsymbol{\tau}_k]\}. \tag{16}$$

However, with the particular choice of regulator we make, $\delta(\mathbf{r}) \to \delta_{R_{3N}}(\mathbf{r}) \propto \mathrm{e}^{-(r/R_{3N})^4}$, this freedom is broken, and some sensitivity to the choice of operator in Eq. (16) remains. We have explored three options:

$$V_{E\tau} \propto \sum_{i<j<k} \sum_{\text{cyc}} \boldsymbol{\tau}_i{\cdot}\boldsymbol{\tau}_k\, \delta_{R_{3N}}(\mathbf{r}_{ij})\, \delta_{R_{3N}}(\mathbf{r}_{kj}), \tag{17}$$

$$V_{E\mathbb{1}} \propto \sum_{i<j<k} \sum_{\text{cyc}} \delta_{R_{3N}}(\mathbf{r}_{ij})\, \delta_{R_{3N}}(\mathbf{r}_{kj}), \tag{18}$$

$$V_{E\mathcal{P}} \propto \sum_{i<j<k} \sum_{\text{cyc}} \mathcal{P}\, \delta_{R_{3N}}(\mathbf{r}_{ij})\, \delta_{R_{3N}}(\mathbf{r}_{kj}), \tag{19}$$

with the projector

$$\mathcal{P} = \frac{1}{36}\Big(3 - \sum_{i<j} \boldsymbol{\sigma}_i{\cdot}\boldsymbol{\sigma}_j\Big)\Big(3 - \sum_{k<l} \boldsymbol{\tau}_k{\cdot}\boldsymbol{\tau}_l\Big) \tag{20}$$

onto triples with total spin $S = \frac{1}{2}$ and total isospin $T = \frac{1}{2}$. These are the triples that would survive in the infinite momentum-space cutoff limit.

## 3.2 Fits and results

The LECs appearing in Fig. 1, $c_1$, $c_3$, and $c_4$, are already set in the pion-nucleon sector. However, the LECs $c_D$ and $c_E$ first appear in the three-nucleon sector at $\mathrm{N^2LO}$ and must be fitted to some three- (or more-) body observables. An important consideration is to fit to uncorrelated observables. In the past, properties of $A = 3$ and $A = 4$ nuclei have been used to fix $c_D$ and $c_E$. The shortcoming of this approach, however, is that largely, if one obtains reasonable properties of $A = 3$ nuclei, then the properties of the $A = 4$ nucleus are typically reproduced well: the two systems are highly correlated. In addition, we have two other motivations for our choices. The first motivation is to probe properties of light nuclei. For this reason, we choose the $^4$He binding energy as one observable. The second motivation is to probe the $T = 3/2$ physics. For this reason, we choose to reproduce $n$–$\alpha$ elastic scattering $P$-wave phase shifts. See Ref. [12] for details on the scattering calculations. The $n$–$\alpha$ system is the lightest known nuclear system where three neutrons may interact and therefore probes the $T = 3/2$ physics. Figure 2 shows the fits we performed. The top panel shows contours of $c_E$ vs $c_D$. Each point in this panel corresponds to values of $c_D$ and $c_E$ for a given operator combination (e. g., $V_{D2}$ and $V_{E\tau}$), for a given cutoff $R_0$ which gives

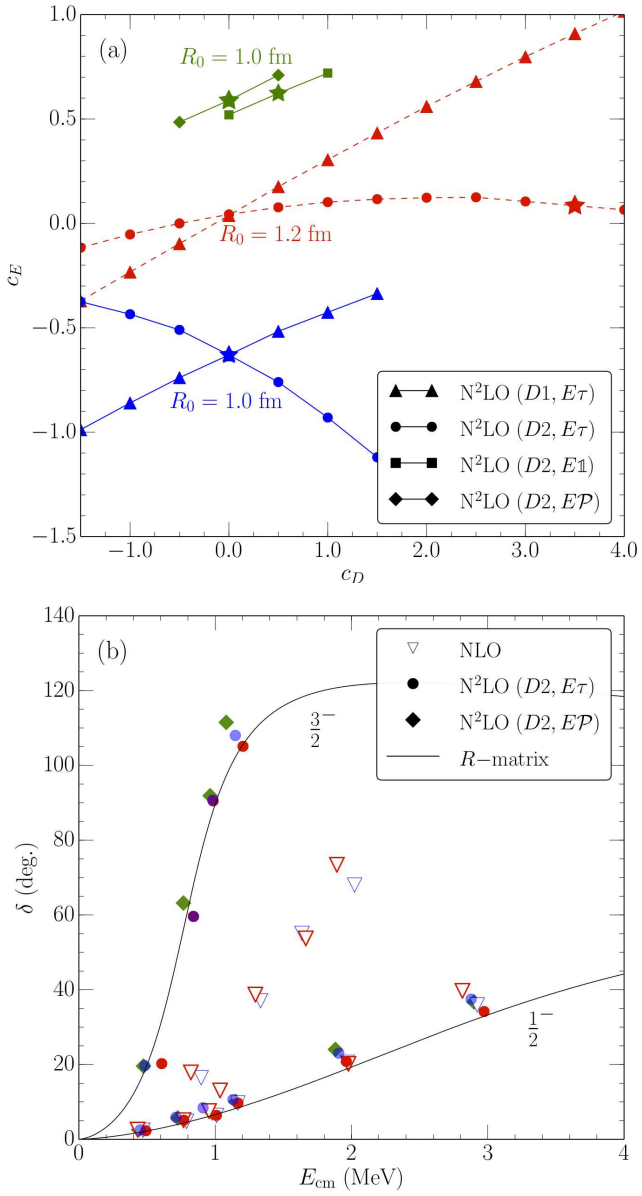


Figure 2: Top panel: Couplings $c_E$ vs $c_D$ obtained by fitting the $^4$He binding energy for different $3N$-operator forms. Triangles are obtained by using $V_{D1}$ and $V_{E\tau}$, other symbols are obtained for $V_{D2}$ and three different $V_E$-operator structures. The blue and green curves correspond to $R_0 = 1.0$ fm, the red curves correspond to $R_0 = 1.2$ fm. The GFMC statistical errors are smaller than the symbols. The stars correspond to the $c_D$ and $c_E$ values which simultaneously fit the $n$–$\alpha$ $P$-wave phase shifts. No fit to both observables can be obtained for the case with $R_0 = 1.2$ fm and $V_{D1}$. Bottm panel: $P$-wave $n$–$\alpha$ elastic scattering phase shifts compared with $R$-matrix analysis of experimental data. The same colors and symbols are used to distinguish the operator combinations. We include also the phase shifts calculated at NLO clearly indicating the necessity of $3N$ interactions to fit the $P$-wave splitting.

the experimental binding energy of $^4$He in GFMC calculations. The stars in the left panel indicate values of $c_D$ and $c_E$ which simultaneously fit the $^4$He binding energy and the $P$-wave elastic $n$–$\alpha$ scattering phase shifts shown in the bottom panel. A good description of both systems is obtained for both cutoffs ($R_0 = 1.0$ fm and $R_0 = 1.2$ fm) for the operator combinations $V_{D2}$ and any of $V_{E\mathbb{1}}$, $V_{E\tau}$, or $V_{E\mathcal{P}}$ (though only the cases with $V_{E\tau}$ and $V_{E\mathcal{P}}$ are shown in Fig. 2). Whereas for the operator combinations with $V_{D1}$ and the softer cutoff $R_0 = 1.2$ fm, no fit to the $P$-wave $n$–$\alpha$ elastic scattering phase shifts could be obtained.

The interactions fit as just described, were used in GFMC calculations of light nuclei (top panel of Fig. 3) and in AFDMC calculations of the equation of state of neutron matter (bottom panel of Fig. 3). The uncertainties shown in Fig. 3 are obtained as a sum in quadrature of the QMC statistical uncertainties and a systematic estimate of the uncertainty induced by truncating the chiral expansion as in Ref. [13]. In short, taken together, Fig. 2 and Fig. 3 imply that our local N$^2$LO interactions have the freedom to simultaneously describe three benchmark nuclear systems: light nuclei, $n$–$\alpha$ elastic scattering phase shifts, and the neutron matter equation of state.

## 4 Application: neutrons in finite volume

Though QCD is the correct theory underlying the strong interactions, the only *ab initio* method to solve it directly at low energies is lattice QCD. Significant progress has been made in these simulations in the last two decades; however, even optimistically the simulation of $^{12}$C in terms of quark and gluon degrees of freedom at physical pion masses is likely in a distant future. Therefore, some connection between the lattice QCD and *ab initio* calculations of nuclear systems in terms of nucleon and pion degrees of freedom is desirable. For example, it is conceivable that in the near future, matching of lattice QCD calculations to chiral Hamiltonians will allow for the extraction of LECs needed for chiral Hamiltonians from lattice QCD simulations. To help facilitate the construction of such a bridge, we have used the AFDMC method to calculate properties of two neutrons in a box with periodic boundary conditions and used the Lüscher formula to extract scattering properties (the scattering length $a$ and effective range $r_\mathrm{e}$) from our finite-volume calculations. For details, see Ref. [14]; here we summarize the main findings.

This work takes advantage of the formalism first introduced by Lüscher [15, 16] relating scattering phase shifts in infinite volume directly to the energy levels in finite volume. The relationship has some remarkable implications. For example, take a simple scattering problem, such as $np \to d\gamma$ radiative capture in the $^1S_0$ channel. One might naively expect that in order to simulate this problem in finite volume it would require cubic volumes with side lengths $L \gg |a^{^1S_0}|, |a^{^3S_1}|$, with, e. g., $a^{^1S_0} = -23.71$ fm. However, this is not so. The Lüscher relationship

$$p \cot \delta_0(p) = \frac{1}{\pi L}\, S\left[\left(\frac{Lp}{2\pi}\right)^2\right], \tag{21}$$

with the regulated sum

$$S(\eta) \equiv \lim_{\Lambda_j \to \infty} \left( \sum_{\mathbf{j}}^{\Lambda_j} \frac{1}{|\mathbf{j}|^2 - \eta} - 4\pi\Lambda_j \right), \tag{22}$$

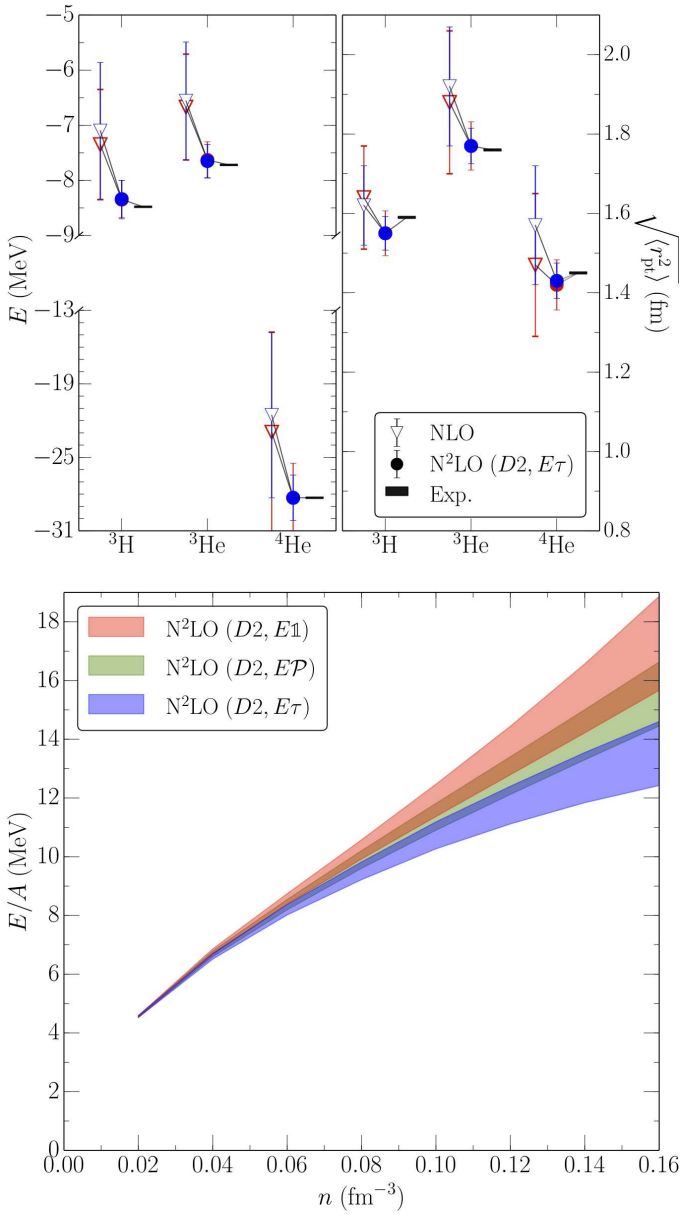


Figure 3: Top panel: Ground-state energies and point proton radii of $A = 3, 4$ nuclei calculated at NLO and N$^2$LO (with $V_{D2}$ and $V_{E\tau}$) compared with experiment. Blue (red) symbols correspond to $R_0 = 1.0$ fm ($R_0 = 1.2$ fm). The errors are obtained as described in the text and include also the GFMC statistical uncertainties. Bottom panel: The energy per particle in neutron matter as a function of density for the $NN$ and full $3N$ interactions at N$^2$LO with $R_0 = 1.0$ fm. We use $V_{D2}$ and different $3N$ contact structures: the blue band corresponds to $V_{E\tau}$, the red band corresponds to $V_{E\mathbb{1}}$, and the green band corresponds to $V_{E\mathcal{P}}$. The green band coincides with the $NN + 2\pi$-exchange-only result because both $V_D$ and $V_E$ vanish in this case. The bands are calculated as described in the text.

(with some caveats) relates the phase shifts $\delta_0(p)$ to the finite-volume spectrum (given by the discrete values of $p$) even for $L < |a^{^1S_0}|$ or other relevant scales. In the above, $\mathbf{j}$ is a vector of integers, and $\Lambda_j$ is a cutoff such that $|\mathbf{j}| < \Lambda_j$. In particular, for low-energy $S$-wave scattering, one can expand the left-hand side of Eq. (21) to obtain a relationship between the scattering parameters of the two-neutron system and the finite-volume spectrum:

$$-\frac{1}{a^{^1S_0}} + \frac{1}{2} r_{\rm e}^{^1S_0} p^2 = \frac{1}{\pi L}\, S\left[\left(\frac{Lp}{2\pi}\right)^2\right]. \tag{23}$$

We first consider only a contact interaction (smeared out),

$$V(r) = C_0\, \mathrm{e}^{-(r/R_0)^4}, \tag{24}$$

which purposely has the same form as the regulated contact interactions we use in our chiral EFT interactions. We introduce a dimensionless variable $q \equiv pL/2\pi$, and calculate the finite-volume ground state for two values of $C_0$. The first value reproduces the physical scattering length in the infinite volume, and the second produces a large scattering length $a = -101.7$ fm. In addition, we calculate the first excited state for the case which gives the physical scattering length, see Fig. 4. From these calculations, we can verify via Eq. (23) that our finite-volume spectra lie along the line predicted by the Lüscher formula with the appropriate scattering length and effective range (calculated in the infinite volume), and in kind, we can take the finite-volume spectra and fit them via Eq. (23) to make a postdiction of the scattering length and effective range. In the case of the large scattering length, this fitting procedure gives $a = -98(4)$ fm compared with the value of $a = -101.7$ fm from the infinite volume. In the case of the physical scattering length, we find $a = -19.0(1)$ fm compared with $a = -18.9$ fm from the infinite volume calculations.

The bottom panel of Fig. 4 shows the first AFDMC calculations of an excited state of a nuclear system. The details are described in Ref. [14]; briefly, we first considered the possibility of introducing a purely spherical node in the Jastrow wave function (points given as red circles in the bottom panel of Fig. 4). However, we also diagonalized the system exactly and from this diagonalization extracted the nodal surface of the first excited state. This nodal surface showed itself to be a linear combination of cubical harmonics with a large spherical component, but with a non-negligible $Y^c_{l=4}$ component as well ($Y^c_l$ is a cubical harmonic). To account for this discrepancy, we estimated the contribution from the non-spherical part of the wave function to contribute an additional 1% uncertainty in the energies we calculated. These are the larger error bars on the red circles in the bottom panel of Fig. 4. When we take this deformed nature of the nodal surface into account in our wave function (yellow squares in the right panel of Fig. 4), a significantly better agreement with the diagonalization and Lüscher formula is obtained.

We then included our local chiral EFT interactions up to N$^2$LO. One caveat to this procedure is that Lüscher's derivation was in terms of a pionless EFT with contact-only interactions. Once the interaction involves the exchange of pions and a larger range, one needs to restrict the momenta used in the comparison to the radius of convergence of pionless EFT $|p| < m_\pi/2$. This excluded region is indicated in Fig. 5 and Fig. 6 by the gray shading, and furthermore, points in this region are not used in the subsequent fitting procedure to determine the scattering lengths and effective ranges.

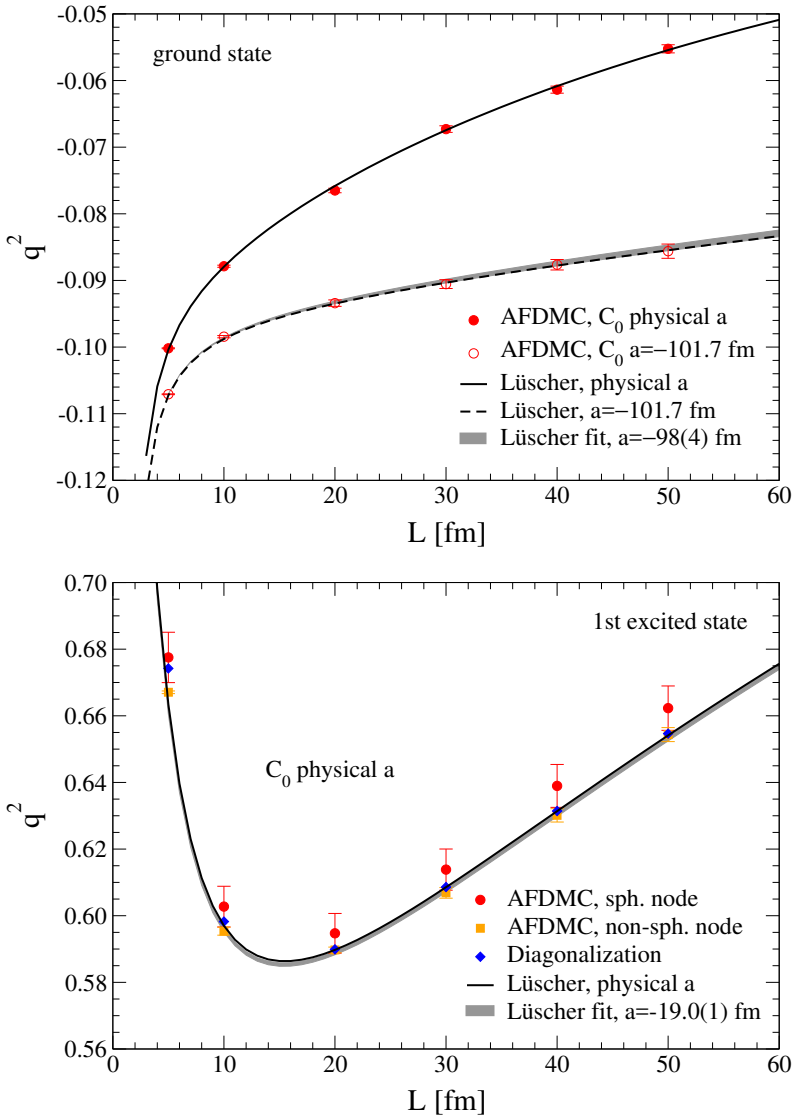


Figure 4: Top panel: AFDMC results for the energy of two neutrons in the ground state in finite volume with the contact potential Eq. (24) for different box sizes $L$ compared with the Lüscher formula. $C_0$ is adjusted to give the physical $nn$ scattering length $a = -18.9$ fm (closed circles/solid line) and to give a very large scattering length $a = -101.7$ fm (open circles/dashed line). The gray band shows a fit (as described in the text) to the AFDMC results for $a = -101.7$ fm. The energies are given in terms of the dimensionless quantity $q^2 = EML^2/(4\pi^2)$. Bottom panel: AFDMC results for the energy of two neutrons in the first excited state in finite volume with the contact potential for different box sizes $L$ (red circles) compared with the Lüscher formula (solid line). The error bars of the AFDMC results with a spherical nodal surface include both statistical uncertainties and a systematic uncertainty of 1% discussed in the text. $C_0$ is adjusted to give the physical $nn$ scattering length $a = -18.9$ fm. Also shown are the energies calculated by exact diagonalization (blue diamonds).

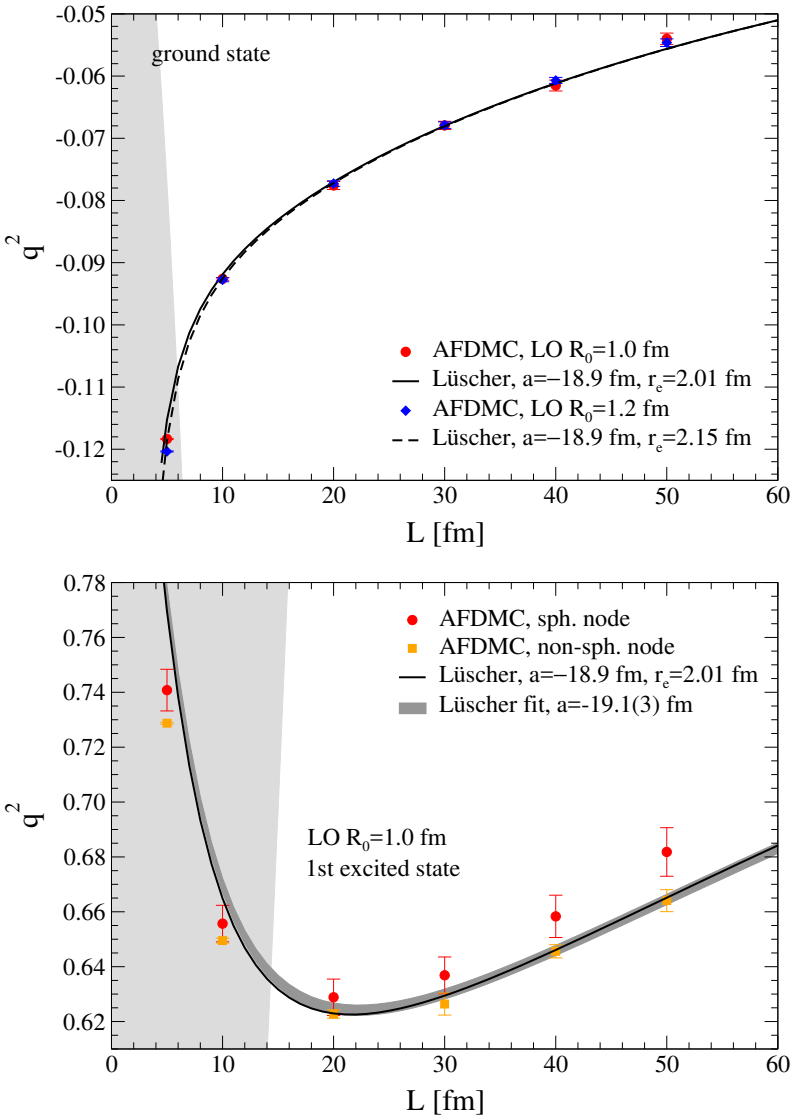


Figure 5: Top panel: AFDMC results for the energy of two neutrons in the ground state in finite volume with the LO chiral EFT interaction compared with the Lüscher formula for different box sizes $L$. The cutoffs $R_0 = 1.0$ fm (red circles/solid line) and $R_0 = 1.2$ fm (blue diamonds/dashed line) are used. The energies are given in terms of the dimensionless quantity $q^2 = EML^2/(4\pi^2)$. The region where $|p| > m_\pi/2$ is indicated by the gray band. Bottm panel: AFDMC results for the energy of two neutrons in the first excited state in finite volume with the LO chiral EFT interaction with cutoff $R_0 = 1.0$ fm (red circles) compared with the Lüscher formula (solid line) for different box sizes $L$. The error bars on the AFDMC results with a spherical nodal surface include both statistical uncertainties and a systematic uncertainty of 1% discussed in the text. The dark gray band shows a combined fit (as described in the text) to the ground and first excited state AFDMC results for the LO chiral potential. Points in the region $|p| > m_\pi/2$ indicated by the gray band are not included in the fit.

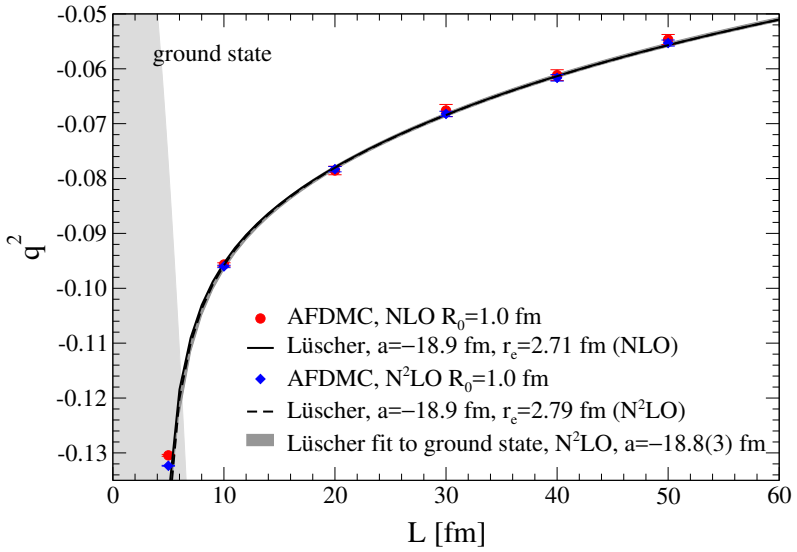


Figure 6: AFDMC results for the energy of two neutrons in the ground state in finite volume with the NLO and N$^2$LO chiral EFT interactions with cutoff $R_0 = 1.0$ fm compared with the Lüscher formula for different box sizes $L$. The results at NLO (N$^2$LO) are given as the red circles/solid line (blue diamonds/dashed line). The dark gray band shows a fit (as described in the text) to the AFDMC results for the N$^2$LO chiral potential. The energies are given in terms of the dimensionless quantity $q^2 = EML^2/(4\pi^2)$. Points in the region $|p| > m_\pi/2$ indicated by the gray band are not included in the fit.

In summary, this application establishes the AFDMC method as a powerful way to match lattice QCD results to finite-volume calculations using chiral Hamiltonians. This procedure has several advantages, including the fact that it circumvents the small-volume and multi-body difficulties of direct Lüscher extensions. In the future, we hope to collaborate directly with the lattice QCD community and extract LECs directly from lattice simulations of few-nucleon systems.

## 5 Conclusion

The advent of QMC calculations combined with chiral EFT interactions is a significant advancement, which can yield new insights into both nuclear interactions and nuclear systems. Our results suggest that more investigation of regulator choices and effects are necessary. Our results also affirm that chiral two- and three-nucleon interactions at N$^2$LO have sufficient freedom to give a good description of light nuclei, $n$–$\alpha$ scattering, and neutron matter. The application shown above demonstrates the exciting connections to diverse other fields that are now possible. The future includes many interesting directions including calculations of larger nuclear systems up to $A = 12$ with the GFMC method, and perhaps beyond with the AFDMC method. One important extension will be to apply our $n$–$\alpha$ scattering framework to other reactions in light nuclei. Low-energy nuclear theory can make significant contributions to many

areas of physics and the combination of chiral EFT in QMC calculations can play an important role.

## References

[1] E. Epelbaum, H.-W. Hammer and U.-G. Meißner, Rev. Mod. Phys. **81**, 1773 (2009).

[2] R. Machleidt and D. R. Entem, Phys. Rep. **503**, 1 (2011).

[3] J. E. Lynn and K. E. Schmidt, Phys. Rev. C **86**, 014324 (2012).

[4] A. Roggero, A. Mukherjee and F. Pederiva, Phys. Rev. Lett. **112**, 221103 (2014).

[5] A. Gezerlis, I. Tews, E. Epelbaum, M. Freunek, S. Gandolfi, K. Hebeler, A. Nogga and A. Schwenk, Phys. Rev. C **90**, 054323 (2014).

[6] I. Tews, S. Gandolfi, A. Gezerlis and A. Schwenk, Phys. Rev. C **93**, 024305 (2016).

[7] J. E. Lynn, J. Carlson, E. Epelbaum, S. Gandolfi A. Gezerlis, and A. Schwenk, Phys. Rev. Lett. **113** 192501 (2014).

[8] J. E. Lynn, I. Tews, J. Carlson, S. Gandolfi, A. Gezerlis, K. E. Schmidt and A. Schwenk, Phys. Rev. Lett. **116** 062501 (2016).

[9] M. Piarulli, L. Girlanda, R. Schiavilla, R. Navarro Pérez, J. E. Amaro and E. Ruiz Arriola, Phys. Rev. C **91**, 024003 (2015).

[10] S. A. Coon and H. K. Han, Few-Body Syst. **30**, 131 (2001).

[11] J. Fujita and H. Miyazawa, Progr. Theor. Phys. **17**, 360 (1957).

[12] K. M. Nollett, S. C. Pieper, R. B. Wiringa, J. Carlson and G. M. Hale, Phys. Rev. Lett. **99**, 022502 (2007).

[13] E. Epelbaum, H. Krebs and U. G. Meißner, Eur. Phys. J. A **51**, 53 (2015).

[14] P. Klos, J. E. Lynn, I. Tews, S. Gandolfi, A. Gezerlis, H.-W. Hammer, M. Hoferichter and A. Schwenk, Phys. Rev. C **94**, 054005 (2016).

[15] M. Lüscher, Commun. Math. Phys. **105**, 153 (1986).

[16] M. Lüscher, Nucl. Phys. B **354**, 531 (1991).